Received 17 October 2023; revised 6 February 2024 and 27 February 2024; accepted 28 February 2024. Date of publication 5 March 2024; date of current version 1 April 2024. The review of this article was arranged by Editor C.-M. Zetterling.

Digital Object Identifier 10.1109/JEDS.2024.3372596

Characteristics Comparison of SiC and GaN Extrinsic Vertical Photoconductive Switches

LINGLONG ZENG[1,2], LANGNING WANG[1,2], XINYUE NIU[1,2], FUYIN LIU[1,2], TING HE[1,2], YANRAN GU[1,2], MUYU YI[1,2], JINMEI YAO[1,2], TAO XUN[1,2], AND HANWU YANG[1,2]

1 College of Advanced Interdisciplinary Studies, National University of Defense Technology, Changsha 410073, China.
2 Nanhu Laser Laboratory, National University of Defense Technology, Changsha 410073, China.

CORRESPONDING AUTHORS: L. WANG AND T. XUN (e-mail: wanglangning@126.com; xtao_0301@hotmail.com)

This work was supported in part by the National Natural Science Foundation of China under Grant 62071477 and Grant 62101577, and in part by the Natural Science Foundation of Hunan Province under Grant 2021JJ40660.

ABSTRACT Vertical extrinsic photoconductive semiconductor switches (PCSSs) are presented with initial characteristics comparison between V-doped 4H-SiC and Fe-doped GaN PCSS under axial triggering such as dark resistance, photoconductivity, power output, and breakdown behavior. Experiments are carried out under the 532-nm-wavelength laser with mJ-level energy and a pulse width of 30 ns. Photoconductive experiments show that the photoelectric conversion efficiency of GaN PCSS is 2.27 times higher than 4H-SiC PCSS with the same electric field strength under different laser energies from 1 mJ to 5 mJ. 4H-SiC PCSS with a dark-state resistance of 10^{12} Ω· cm can withstand a bias voltage of 8 kV (16 kV/mm) and laser energy of 8 mJ and the maximum output power is up to 428.7 kW, while that of GaN can only stand a bias voltage of 1 kV (2.9 kV/mm) because of low dark resistance and defect. Obvious cracks of 4H-SiC PCSS can be observed from the breakdown image after breakdown occurs, while the dark-state resistance of GaN PCSS drops from 10^6 Ω· cm to 10^4 Ω· cm under high DC voltage.

INDEX TERMS Photoconductive semiconductor switch, silicon carbide, gallium nitride, breakdown, photoelectric conversion efficiency, output power.

I. INTRODUCTION

Photoconductive semiconductor switches (PCSSs) have an attractive application with the characteristic of fast response, low switch jitter, and high power [1], [2], which has been widely used in ultra-fast electronics (ps/THz), power microwave/RF sources (MW), solid-state pulsed power sources, novel accelerators and so on [3], [4], [5], [6], [7], [8]. PCSS is a two-electrode device with a bulky semiconductor substrate and the characteristics of device are mainly depend on the material characteristics. The third-generation semiconductor materials (SiC, GaN) have many excellent characteristics such as wide bandgap (>3 eV), high carrier saturation velocity ($\sim 2\times10^7$ cm/s), high critical breakdown electric field (MV/cm), and high thermal conductivity [9], which contributes PCSS to operating under high voltage, high frequency and high temperature conditions. By the development of semiconductor material technology, researchers pay attention on third generation semiconductor materials for PCSS, representative materials of SiC and GaN. The different material characteristics make the different performance of PCSS composed of different materials [9], [10], [11], [12], [13], [14].

SiC or GaN PCSSs can be used to operate in intrinsic or extrinsic absorption. Intrinsic excitation occurs when photon energy is greater than the bandgap, and the absorption depth is very shallow (μm or 10 μm level) [13]. 355-nm-wavelength laser (triple frequency of Nd:YAG 1064 nm wavelength) is widely used to illuminate lateral intrinsic PCSS with electrodes on the same side of the substrate [14]. For lateral intrinsic PCSS, a high-charge density is concentrated on the illumination surface with μm level depth when devices are worked in power condition such like kV voltage and 100 A or larger. Xiao et al. fabricated lateral intrinsic SiC PCSS with a bias of 6 kV and 100 A peak current with 3151 times lifetime. However, the uneven distribution of current and electric field enhancement makes it easier to surface flashover breakdown, so it's hard to generate high power pulse for a long lifetime [15].

Extrinsic absorption occurs when the photon energy is smaller than the bandgap. Vertical PCSS with electrodes on opposite side of the substrate are widely illuminated by an extrinsic laser such as waveleng of 532 nm (double frequency of Nd:YAG 1064 nm wavelength) [16], [17]. The breakdown voltage of vertical PCSS is high for the thick substrate ~mm dimension level, and the current density can be controlled with a large current cross section since the electrode of vertical power PCSS is about mm-cm dimension. So, it can make full use of high breakdown field properties of bulk materials and assure the bulky current flow [18]. V-doped SiC PCSS can achieve extrinsic absorption through impurity absorption [9], and researchers have paid attention on vertical SiC PCSS with extrinsic 532-nm-wavelength laser in terms of high output power, high photoelectric conversion efficiency, and so on [16], [17], [18]. Sullivan has reported that the power capacity of a single thickness of 1 mm and side width of 1 cm square SiC wafer is 22.4 MW (16 kV bias voltage and 1.4 kA peak current) with a 5 MW peak optical power input [9].

Extrinsic lasers can be incident from the narrow side facet of or through the electrode vertically (axial-triggering) for vertical PCSSs illumination [19]. The axial-triggering vertical SiC PCSS with transparent electrode and mirror electrode is considered a promising candidate for high-power SiC PCSSs, as the current and electric field are distributed uniformly in the inner area and less photocurrent passes through near the electrode area (high electric area) [18]. Previously, we have optimized the electrode of the axial triggering SiC PCSS, which can continuously output electrical pulses for 10 minutes at a 100 Hz repetition rate, 30-ns pulse width, DC voltage bias 16.5 kV/mm and 100 A peak current without breakdown [16].

GaN PCSS research is primarily conducted by Sullivan [9], Leach et al. [22], Mauch et al. [12], [21], and Hu et al. [23], [24]. In previous studies, lateral GaN PCSS optical and electrical properties were studied with different geometries for high voltage applications [11], [20], [21]. Investigation on the output performance of vertical GaN PCSS in side irradiation at high voltage had also been conducted in simulation and experiment with micro-joule triggering laser energy for ps-level switching [22], [23], [24]. However, few researches on the output characteristics of vertical GaN PCSS are conducted with axial triggering, and little experimental comparison is made on vertical axial triggering 4H-SiC and GaN PCSSs' output characteristics. In this paper, initial comparison and analysis of vertical 4H-SiC and GaN PCSSs output characteristics were conducted at the extrinsic laser wavelength of 532 nm.

II. MATERIALS AND STRUCTURES OF DEVICES

The vertical structure of 4H-SiC or GaN PCSS is shown in Fig. 1. Al-doped ZnO (AZO) transparent conductive film is coated on the light incident surface. AZO has excellent optical with high transmittance and electrical properties with low resisitivity (10^{-4} Ω·cm). As the electrode of the

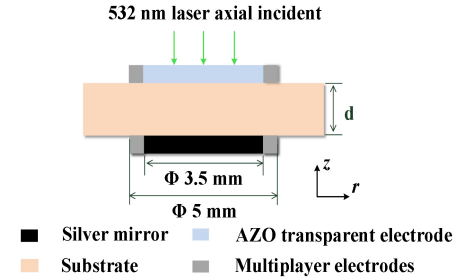

FIGURE 1. Vertical PCSS structure under axial triggering.

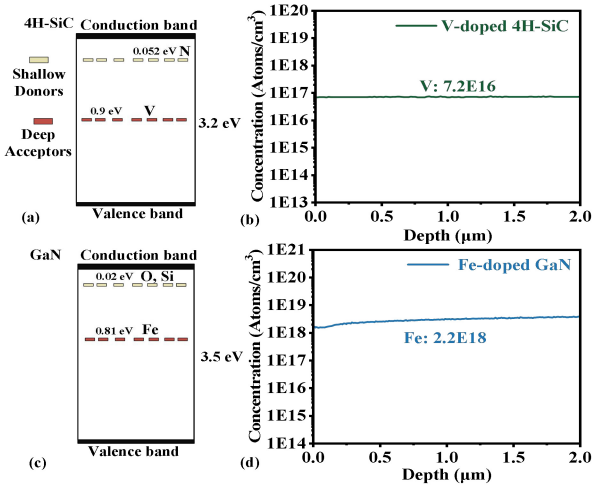

FIGURE 2. Energy level of major impurities in (a) 4H-SiC and (b) the doping concentration of V in 4H-SiC with different depth (0-2 μm), (c) energy level of major impurities in GaN and (b) the doping concentration of Fe in GaN with different depth (0-2 μm) [9], [25].

PCSS providing conductive channel, it has the effect of anti-reflection to enhance the laser absorption and reduce reflective losses. Ag is coated on the exit surface of light to enhance the reflection, prolong the optical path of light transmission and increase the absorption of laser in the substrate. Circular electrodes are coated on the incident and exit planes, the inside and outside diameter of the ring are 3.5 mm and 5 mm respectively. Substrate of PCSS is 12 mm × 12 mm, and d represents the thickness of the substrate. Fig. 2 shows the energy level of major impurities of substate (4H-SiC and GaN).

A. SUBSTRATE: V-DOPED SIC

SiC PCSS is fabricated on a standard 4H-SiC wafer with 0.5 mm thickness ($d_1 = 0.5$ mm). The wafer is manufactured by Guangzhou Summit Crystal Semiconductors Co., Ltd, using Physical Vapor Transport (PVT) method. We use the Secondary Ion Mass Spectrometry (SIMS) method to obtain the major impurity density in 4H-SiC. The concentration of V is 7.2×10^{16} cm^{-3}, and impurities N is 3.7×10^{16} cm^{-3}, other impurities like Al, B, Ti are lower than 1×10^{16} cm^{-3}. Energy levels and the doping concentration of V in 4H-SiC with different depth (0-2 μm) are shown in Fig. 2(a) and (b). First, deep acceptor level $V^{3+/4+}$ can compensate

shallow donor level N, the Fermi level is far away from the conduction and valence bands. The concentration of free carriers is very low, achieving semi-insulation characteristic, the dark state resistance of the semi-insulating 4H-SiC PCSS is measured by ST2643 high resistance meter (Suzhou Jingge Electronic Co., Ltd) and it is 10^{12} Ω·cm. Second, 4H-SiC PCSS can achieve extrinsic absorption through impurity absorption when the photon energy of the 532 nm laser (2.33 eV) used in the experiment is lower than the bandgap energy of 4H-SiC (3.2 eV).

B. SUBSTRATE: FE-DOPED GAN

Suzhou Nanowin Science and Technology Co., Ltd provide standared Fe-doped semi-insulating GaN with a thickness of 0.35 mm (d_2=0.35 mm). GaN wafers are manufactured using Hydride Vapor Phase Epitaxy (HVPE). By the measurement of SIMS, impurities O (2.1×10^{16} cm^{-3}) and Si (5.3×10^{16} cm^{-3}) are introduced in the substrate. Fe is intentionally compensated into GaN, the doping concentration of Fe is 2.2×10^{18} cm^{-3}, their energy levels and the doping concentration of Fe in GaN with different depth (0-2 μm) are shown in Fig. 2(c) and (d). First, Fe deep-level acceptor will compensate for O and Si shallow-level donors to form semi-insulation characteristic. The measured dark-state resistance of the semi-insulating GaN PCSS is 10^6 Ω·cm, which is 6 orders of magnitude lower than the dark state resistance of 4H-SiC. Many columnar defects will be introduced in the growth of GaN in HVPE leading to lower resistivity. Second, the photon energy of 532 nm is lower than the bandgap energy of GaN (3.5 eV), the extrinsic light absorption property can be achieved through impurity absorption.

III. EXPERIMENTAL SETUP AND TYPICAL WAVEFORMS

Fig. 3(a) and (b) is the experimental platform of PCSS, the circuit consists of six 30 kV/1nF high-voltage ceramic storage capacitors, one 4H-SiC/GaN PCSS, two 30 dB attenuators (Huaxiang/SHX MS2-8000, Shanghai, China) and an oscilloscope (LeCroy WR9404M, New York, America). The capacitors act as DC voltage source with discharge time constant longer than carrier lifetime. The characteristic impedance of the attenuator in the circuit is 50 Ω, the output voltage attenuated 1000 times is measured by the oscilloscope. The laser is generated from a double frequency of Q-switched Nd:YAG laser with an output pulse of 30 ns at full-wave-at-half-maximum (FWHM), the energy of 532 nm laser ranges from 1 mJ to 8 mJ. The voltage of DC source ranges from 0 to 10 kV. When the bias loaded on the switch is changed (4H-SiC PCSS: 200 V, 600 V, 1000V; GaN PCSS: 300 V, 500 V, 700 V), the typical output waveform of 4H-SiC and GaN when laser pulse energy is 1 mJ (~33 kW) is shown in Fig. 4(a) and (b). The output voltage amplitude of the circuit where the 4H-SiC and GaN PCSS are located will increase with the increase of the bias voltage.

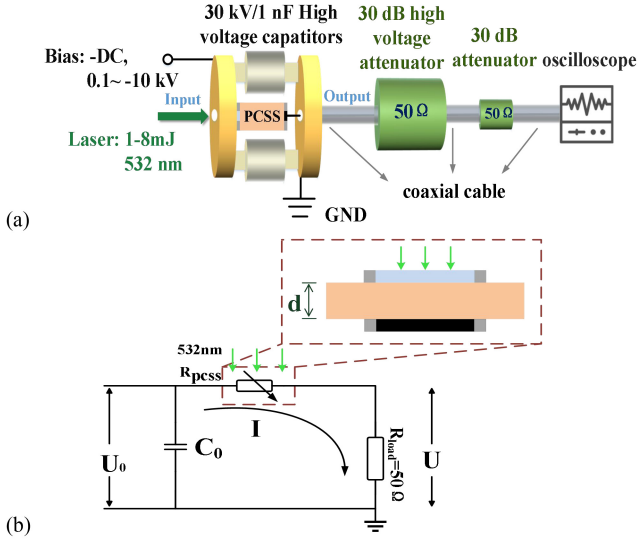

FIGURE 3. (a) Experimental platform structure and (b) simplified circuit schematic.

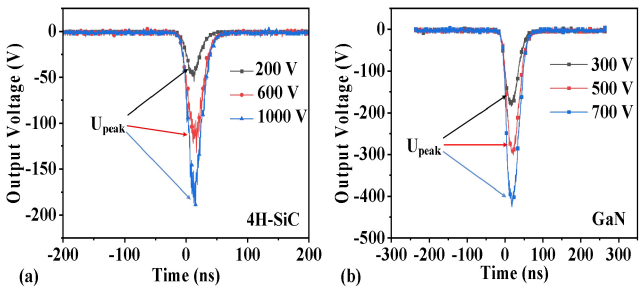

FIGURE 4. Typical waveforms of (a) 4H-SiC and (b) GaN output voltage varying with bias voltages (4H-SiC: 200 V, 600 V, 1000 V; GaN: 300 V, 500 V, 700 V) at 1 mJ.

IV. COMPARATIVE EXPERIMENTAL RESULTS

A. PHOTOCONDUCTIVITY TEST RESULTS UNDER DIFFERENT BIAS VOLTAGES AND LASER ENERGIES

The waveforms from Fig. 4 refer to U_{peak}. It is the maximum value of the output electric pluse. The value of minimum on-state resistance can be calculated according to U_{peak} and circuit structure in Fig. 3(b):

$$I_{peak} = U_{peak}/R_{load} \quad (1)$$

$$R_{pcss} = U_0/I_{peak} - R_{load} \quad (2)$$

$$E_{pcss} = \left(U_0 - I_{peak}R_{load}\right)/d \quad (3)$$

where U_0 is the bias voltage, U_{peak} is the output voltage amplitude, I_{peak} is the current in the circuit, R_{pcss} is the minimum on-state resistance of the switch, R_{load} is the 50 Ω load resistance, E_{pcss} is the electric field intensity of the PCSS when the on-state resistance is minimum.

When the laser energy changes as follows: 1 mJ, 2 mJ, 3 mJ, 4 mJ, and 5 mJ, the change of the peak output voltage with different bias voltage of 4H-SiC and GaN PCSSs are shown in Fig. 5(a) and (b). The different bias voltage of SiC (200V, 400, 600, 800V, 1000V) and GaN (300V, 400, 500, 600, 700V) is to obtain similar electric field intensity for

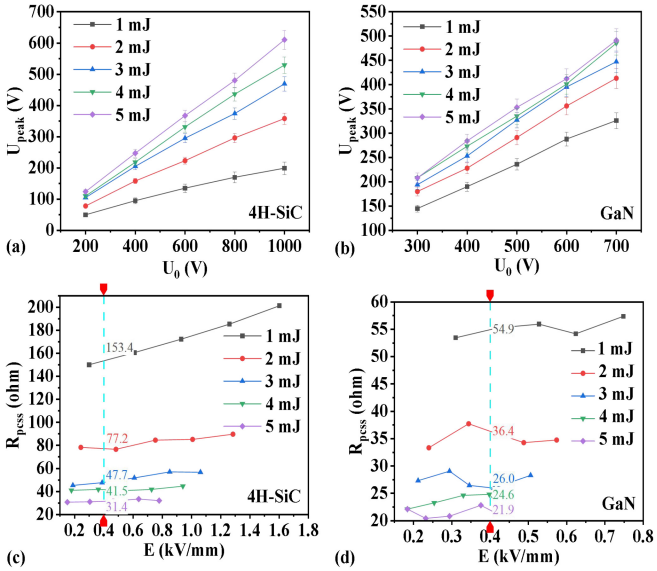

FIGURE 5. The variation of output voltage of (a) 4H-SiC and (b) GaN with different bias voltages (4H-SiC PCSS: 200 V, 400 V, 600 V, 800 V, 1000V; GaN PCSS: 300 V, 400 V, 500 V, 600 V, 700 V) under different laser energies (1 mJ, 2 mJ, 3 mJ, 4 mJ, 5 mJ), the variation of minimum on-state resistance of (c) 4H-SiC and (d) GaN PCSS with different electric fields under different laser energies (1 mJ, 2 mJ, 3 mJ, 4 mJ, 5 mJ).

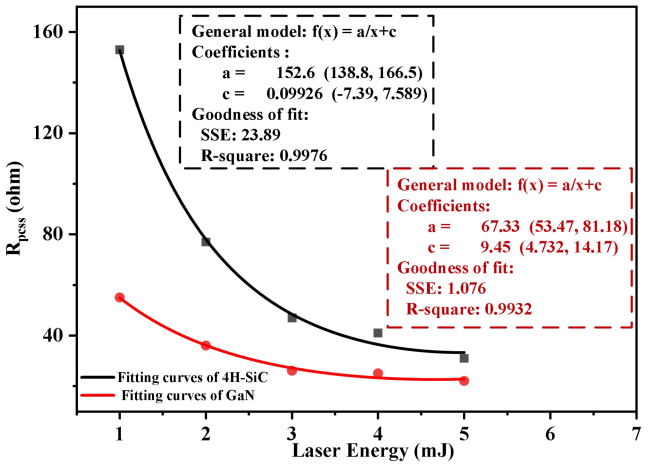

FIGURE 6. Fitting curves of minimum on-state resistance and laser energy of 4H-SiC and GaN PCSSs when electric field intensity is 0.4 kV/mm.

standard commercially prepared SiC and GaN substrates of different thicknesses.

According to Equation (2) and (3), we can obtain the variation of the on-state resistance of 4H-SiC and GaN PCSS with electric field intensity at different laser energies, as shown in Fig. 5 (c) and (d). The on-state resistance of 4H-SiC and GaN PCSSs decreases with the increase of laser intensity and increases with the increase of electric field intensity. Under the same electric field and laser energy, the on-state resistance of GaN PCSS is smaller than that of 4H-SiC PCSS. According to the on-state resistance expression of the PCSS:

$$R_{pcss} \propto \frac{d}{P(t)\tau\mu\alpha\eta} \tag{4}$$

where hv is photon energy, $P(t)$ is incident laser power, τ is carrier lifetime, μ is field dependence carrier mobility, α is absorption coefficient, and η is quantum efficiency.

When the experimental devices and conditions are known, the device characteristic parameters, except for carrier mobility, will not change with the experimental conditions. According to the carrier mobility model in Equation (5) [16], the carrier mobility decreases with the increase of electric field.

$$\mu = \left[1 \Big/ \left(1 + \left(\frac{\mu_0 E}{v_s}\right)^{\beta}\right)\right]^{1/\beta} \mu_0 \tag{5}$$

E is the electric field, v_s is carrier saturation velocity, μ_0 is the low-field electron mobility, β is a dimensionless fitting parameter. We choose the same electric field intensity for comparative analysis of photoelectric conversion efficiency in Fig. 5(c) and (d). When the electric field strength is determined to be 0.4 kV/mm, the field dependence carrier mobility is also constant. Thus, the minimum on-state resistance of Equation (4) can be simplified as follows:

$$R_{pcss} = a/P_{laser} \tag{6}$$

$$a = 1/\tau\mu\alpha\eta \tag{7}$$

Equation (6) shows that the minimum on-state resistance of the PCSS is inversely proportional to the laser power. The on-state resistance is also inversely proportional to laser energy due to the same pulse width of the optical waveform in different laser energy. Therefore, the data can be fitted with the inverse proportional function as shown in Equation (8):

$$Y = a/x + c \tag{8}$$

where x represent laser energies and Y is the on-state resistance of PCSS, a is the photoconductivity of 4H-SiC or GaN PCSS, the smaller a is, the higher the photoelectric conversion efficiency is. The constant c in Equation (8) is introduced to rectify Equation (6) due to the stray parameters in circuit and surface resistance of PCSS, which may cause the theoretical calculated resistance (R_{pcss}) in Equation (2) to be smaller than the actual resistance. When the electric field intensity is 0.4 kV/mm, the minimum on-state resistance of 4H-SiC and GaN PCSSs at different laser energies (1-5 mJ) can be obtained from Fig. 5(c) and (d). The fitting curve for fitting the minimum on-state resistance and laser energy using Equation (8) is shown in Fig. 6:

From Fig. 6, it can be seen that using Equation (8) can well fit the relationship between laser energy and minimum on-state resistance.

The value c in the fitting function of 4H-SiC is only 0.09 and can be ignored, while that of c in the fitting function of GaN is 19.61 and cannot be ignored. This is due to the irregularity of GaN surface crystal structure, which leads to more defects and non-uniformity on the surface, resulting in

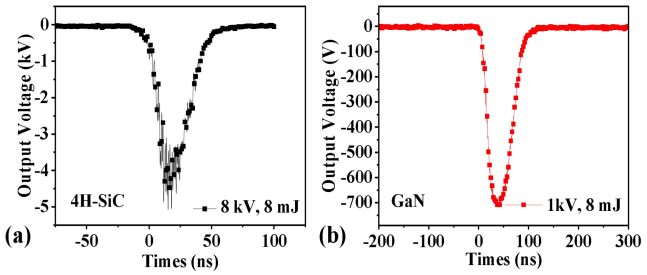

FIGURE 7. Under laser energy of 8 mJ, the electrical waveform of (a) 4H-SiC PCSS at 8 kV and (b) GaN PCSS at 1 kV.

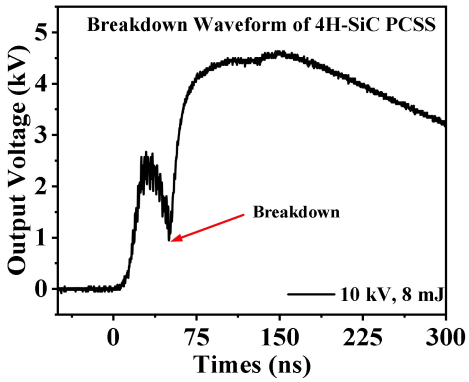

FIGURE 8. The breakdown waveform of 4H-SiC PCSS at 10 kV, 8 mJ.

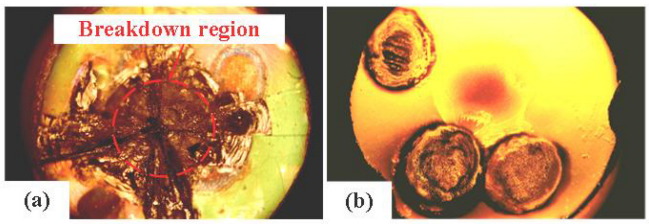

FIGURE 9. Under microscope, (a) 4H-SiC breakdown image at a DC bias voltage of 10 kV, 8 mJ, (b) GaN image at 1 kV, 8 mJ.

greater roughness. There is no good ohmic contact between substrate and electrode, and the contact resistance cannot be ignored, while the ohmic contact between 4H-SiC substrate surface and electrode is good, and the roughness is small. We get the roughness of 4H-SiC and GaN substrates measured by Atomic Force Microscopy. Randomly select the size of 5×5 μm on the switch substrate for measurement and the average roughness of 4H-SiC substrate is only 0.07 nm and that of GaN substrate is 0.77 nm.

While a_1=152.6 of 4H-SiC PCSS, a_2=67.33 of GaN PCSS, a_1/a_2=2.27, the photoelectric conversion efficiency of GaN PCSS is (a_1/a_2=2.27) / (d_1/d_2=1.43) = 1.58 times higher than that of 4H-SiC. The inconsistency between the thickness of 4H-SiC and GaN does not affect the experimental comparison results, which has taken into account the inconsistent thickness of 4H-SiC and GaN substrates. It is the inherent characteristics of GaN material that make its photoelectric conversion efficiency higher than that of 4H-SiC. GaN shows a better performance on the photoelectric conversion efficiency under the same electric field.

B. HIGH POWER PERFORMANCE OF DEVICES UNDER HIGHER BIAS VOLTAGE AND INPUT LASER ENERGY

Continue to increase the DC bias voltage of 4H-SiC to 8 kV and GaN to 1 kV and laser intensity (8 mJ). Their high-power output waveforms are shown in Figs. 7 (a) and (b).

The circuit where 4H-SiC PCSS is located can outputs power of 428.7 kW (4.6 kV, 93 A), while GaN can only withstand 1 kV and the circuit output power is 11.4 kW (760 V, 15 A). The output power of 4H-SiC PCSS is 37.6 times higher than that of GaN PCSS.

In Fig. 7, SiC PCSS have more noise than the GaN device may due to the difference of interstage capacitance of SiC and GaN PCSS, the interstage capacitance of GaN and SiC PCSSs measured by high frequency LCR digital bridge (UC2878A, Changzhou Youce Electronic Technology Co., Ltd.) are 7.3 pF and 5 pF, respectively. The high-frequency response capability of the circuit is mainly affected by the interstage capacitance of the PCSS, GaN PCSS has a larger interstage capacitance and can filter out more high-frequency noise [26].

Continuing increasing the DC bias voltage of 4H-SiC PCSS until breakdown, when the voltage is 10 kV and the laser energy is 8 mJ, the breakdown waveform of 4H-SiC PCSS is shown in Fig. 8. The instantaneous increase of output voltage appears at the falling edge of the electrical pulse waveform, a breakdown channel is formed inside the substrate, the voltage loaded on the PCSS reaches the maximum. While the DC voltage and laser energy of GaN PCSS is 1 kV and 8 mJ, the voltage power was unable to increase due to large leakage current in the loop, the insulation performance of GaN PCSS deteriorates. The images of 4H-SiC at 10 kV, 8 mJ and GaN at 1 kV, 8 mJ were observed under the microscope, as shown in Fig. 9(a) and (b).

The 4H-SiC substrate showed obvious cracks in Fig. 9 and there is obvious carbonization in the center of breakdown. While the transparent electrode in the light-illuminated region of the GaN PCSS shows damage, carbonization and blackness. The breakdown behavior of 4H-SiC and GaN PCSS is different because of different characteristics and breakdown mechanism.

There is no suitable single crystal substrate material for GaN growth, it needs to be grown by heteroepitaxy technology, such as HVPE [27]. If the lattice constant of GaN epitaxy layer is different from that of substrate material, there exists a lattice mismatch problem. Many defects such as columnar and pores will be introduced in the growth process, which will affect the insulation properties of GaN substrate. It is found that the dark resistance of GaN decreases by two orders of magnitude from 10^6 Ω·cm to 10^4 Ω·cm under

DC voltage of 1 kV. At this time, GaN can no longer meet the semi-insulating characteristics. Reducing columnar defects and strain related defects caused by lattice mismatch in the HVPE growth process of GaN is more conducive to improving the insulation characteristics of GaN PCSS under high voltage [20].

C. PHOTOELECTRIC CONVERSION EFFICIENCY UNDER HIGH ELECTRIC FIELD

The photoelectric conversion efficiency of PCSS can be considered as the ratio of the output electrical power to the input optical power:

$$\eta_{\mathrm{OE}} = \frac{P_{out}}{P_{laser}} \tag{9}$$

P_{out} represents the output electrical power, equal to the peak power on the load shown in Fig. 3 (b).

$$P_{out} = U_0^2 R_{load} / \left(R_{load} + R_{pcss}\right)^2 \tag{10}$$

$$U_0 = E_0 d \tag{11}$$

P_{laser} represents the optical peak power of laser pulse, as equation (6) shows. The photoelectric conversion efficiency of PCSS can be analyzed as follows:

$$\begin{aligned}\eta_{\mathrm{OE}} &= \frac{P_{out}}{P_{laser}} \\ &= \frac{U_0^2 R_{load} / \left(R_{load} + R_{pcss}\right)^2}{a / R_{pcss}} \\ &= \frac{U_0^2 R_{load} R_{pcss}}{a\left(R_{load} + R_{pcss}\right)^2} \\ &\le \frac{U_0^2}{4a}\left(R_{load} = R_{pcss}\right)\end{aligned} \tag{12}$$

When $R_{load} = R_{pcss}$, we obtain the biggest photoelectric conversion efficiency. It can be seen from Equation (12) that the photoelectric conversion efficiency is inversely proportional to the photoconductivity. With a relation between U_0 and E_0 and Equation (7), Equation (12) can also be written as follows:

$$\eta_{\mathrm{OE}} \propto E_0^2 \mu \tau \alpha \eta \tag{13}$$

E_0 refers to the electric field intensity on PCSS when the bias voltage is U_0. From Equation (13), to improve the photoelectric conversion efficiency, the electric field E_0, carrier mobility, carrier lifetime, absorption coefficient, and quantum efficiency of PCSS can be improved as follows:

First, the higher the carrier mobility of the material and the electric field intensity of the PCSS, the higher the photoelectric conversion efficiency. We should choose materials with higher electric field strength E_0 and carrier mobility μ as the substrate for PCSS. The theoretical breakdown field strength of GaN (3 MV/cm) is higher than that of 4H-SiC (2.2 MV/cm) [9]. In this experiment, the insulation performance of GaN deteriorates under high voltage, and the working field strength of GaN is lower than that of 4H-SiC. Defects introduced during the growth of GaN limit the operation of GaN PCSS under high electric field intensity.

Second, increasing carrier lifetime τ can increase photoelectric conversion efficiency. However, when the carrier lifetime is too long, it may affect the high-frequency response ability of the PCSS, resulting in longer tail of the output single pulse waveform and poorer modulation of the pulse cluster waveform [28]. The deep-level doping of semiconductor will help to achieve the semi-insulating characteristics of PCSS, but the carrier lifetime will decrease with the increase of doping, thus reducing the photoelectric conversion efficiency of photoconductive switches [29]. Therefore, reasonable doping should be used to regulate the carrier lifetime, so as to increase the photoelectric conversion efficiency while maintaining good frequency response ability.

Third, the absorption coefficient α and the quantum efficiency η refers to the ability of incident light energy to be absorbed by a semiconductor and converted into electrical energy. We can choose to use 1064 or 532 nm laser to change the light absorption coefficient. In addition, we can increase the optical path of light transmission within the substrate by changing the mode of light incidence, such as adding the transparent AZO electrode layer under the Ag mirror to form AZO/SiC/AZO/Ag structure [16] or utilizing light capture structure to form total internal reflection [30], thereby improving the light absorption efficiency. We can also reasonably control the doping concentration so that as many electrons or holes as possible are excited by laser, improving quantum efficiency and finally increasing the photoelectric conversion efficiency [29].

V. CONCLUSION

Preliminarily comparison of the output performance: photoelectric conversion efficiency, maximum output power, and breakdown behavior of 4H-SiC and GaN PCSS are demonstrated in this study. Vertical 4H-SiC and GaN PCSSs are illuminated by a beam of extrinsic 532-nm-wavelength laser under axial triggering, which differs in output characteristics. The results show that GaN PCSS has higher photoelectric conversion efficiency, which is 2.27 times that of 4H-SiC PCSS. However, the 4H-SiC PCSS has stronger voltage resistance with 8 kV (16.5 kV/mm) and can output higher power of 428.7 kW, while GaN can't work properly when DC bias voltage greater than 1 kV (2.9 kV/mm), and the images of the 4H-SiC and GaN PCSSs in high voltage are analyzed, the surface of 4H-SiC substrate have obvious cross cracks, ablation and carbonization occur in the laser irradiated region of GaN substrate. In the future, GaN crystals will have broader application prospects in PCSS by improving the method of growing GaN to reduce defect density and improve the high-voltage insulation characteristic.

REFERENCES

[1] E. Majda-Zdancewicz, M. Suproniuk, M. Pawłowski, and M. Wierzbowski, "Current state of photoconductive semiconductor switch engineering," *Opto-Electron. Rev.*, vol. 26, no. 2, pp. 92–102, May 2018, doi: 10.1016/j.opelre.2018.02.003.

[2] S. K. Mazumder et al., "Overview of wide/ultra-wide bandgap power semiconductor devices for distributed energy resources," *IEEE J. Emerg. Sel. Top. Power Electron*, vol. 11, no. 4, pp. 3957–3982, Aug. 2023, doi: 10.1109/jestpe.2023.3277828.

[3] F. J. Zutavern et al., "Photoconductive semiconductor switch experiments for pulsed power applications," *IEEE Trans. Electron Devices*, vol. 37, no. 12, pp. 2472–2477, Dec. 1990, doi: 10.1109/16.64520.

[4] O. S. F. Zucker, "High-power microwave generation with photoconductors," *J. Lightw. Technol.*, vol. 26, no. 15, pp. 2430–2440, Aug. 2008, doi: 10.1109/JLT.2008.925611.

[5] M. Xu et al., "Pulse compression characteristics of an opposed-electrode nonlinear GaAs photoconductive semiconductor switch at 2 μJ excitation," *IEEE Electron Device Lett.*, vol. 43, no. 5, pp. 753–756, May 2022, doi: 10.1109/LED.2022.3158552.

[6] X. Chu et al., "Wide-range frequency-agile microwave generation up to 10 GHz based on vanadium-compensated 4H-SiC photoconductive semiconductor switch," *IEEE Electron Device Lett.*, vol. 43, no. 7, pp. 1013–1016, Jul. 2022, doi: 10.1109/led.2022.3179292.

[7] L. Hu, J. Su, R. Qiu, and X. Fang, "Ultra-wideband microwave generation using a low-energy-triggered bulk gallium arsenide avalanche semiconductor switch with ultrafast switching," *IEEE Trans. Electron Devices*, vol. 65, no. 4, pp. 1308–1313, Apr. 2018, doi: 10.1109/TED.2018.2802642.

[8] C. Luan, J. Zhao, L. Xiao, Q. Yang, X. Ma, and H. Li, "All solid-state electromagnetic pulse simulator based on the 4H-SiC photoconductive semiconductor switch," *Rev. Sci. Instrum.*, vol. 91, no. 1, Jul. 2020, Art. no. 014701, doi: 10.1063/1.5128450.

[9] J. S. Sullivan and J. R. Stanley, "Wide bandgap extrinsic photoconductive switches," Lawrence Livermore Nat. Lab., Univ. California, Livermore, CA, USA, Rep. 94550, 2013.

[10] K. S. Kelkar, N. E. Islam, C. M. Fessler, and W. C. Nunnally, "Design and characterization of silicon carbide photoconductive switches for high field applications," *J. Appl. Phys.*, vol. 100, no. 12, Dec. 2006, Art. no. 124905, doi: 10.1063/1.2365713.

[11] X. Wang, S. K. Mazumder, and W. Shi, "A GaN-based insulated-gate photoconductive semiconductor switch for ultrashort high-power electric pulses," *IEEE Electron Device Lett.*, vol. 36, no. 5, pp. 493–495, May 2015, doi: 10.1109/LED.2015.2416188.

[12] D. Mauch et al., "Evaluation of GaN:Fe as a high voltage photoconductive semiconductor switch for pulsed power applications," in *Proc. IEEE Pulsed Power Conf.*, 2015, pp. 1–4, doi: 10.1109/PPC.2015.7296989.

[13] X. Sun et al., "Low on-resistance and high peak voltage transmission efficiency based on high-purity 4H-SiC photoconductive semiconductor switch," *IEEE Trans. Power Electron.*, vol. 39, no. 2, pp. 2013–2019, Feb. 2024, doi: 10.1109/TPEL.2023.3320124.

[14] D. Mauch, W. Sullivan, A. Bullick, A. Neuber, and J. Dickens, "High power lateral silicon carbide photoconductive semiconductor switches and investigation of degradation mechanisms," *IEEE Trans. Plasma Sci.*, vol. 43, no. 6, pp. 2021–2031, Jun. 2015, doi: 10.1109/TPS.2015.2424154.

[15] L. Xiao et al., "Effect of electron avalanche breakdown on a high-purity semi-insulating 4H-SiC photoconductive semiconductor switch under intrinsic absorption," *Appl. Opt.*, vol. 57, no. 11, pp. 2804–2808, Apr. 2018, doi: 10.1364/ao.57.002804.

[16] L. Wang et al., "Breakdown and photoconductivity enhancement by mixed reflective Al-doped ZnO/Ag electrode in vertical SiC photoconductive switch," *IEEE Electron Device Lett.*, vol. 44, no. 5, pp. 721–724, May 2023, doi: 10.1109/LED.2023.3263525L.

[17] L. Wang et al., "Effects of high-field velocity saturation on the performance of V-Doped 6H silicon-carbide photoconductive switches," *IEEE J. Emerg. Sel. Top. Power Electron*, vol. 9, no. 4, pp. 4879–4886, Aug. 2021, doi: 10.1109/JESTPE.2020.3038561.

[18] P. Cao, W. Huang, H. Guo, and Y. Zhang, "Performance of a vertical 4H-SiC photoconductive switch with AZO transparent conductive window and silver mirror reflector," *IEEE Trans. Electron Devices*, vol. 65, no. 5, pp. 2047–2051, May 2018, doi: 10.1109/ted.2018.2815634.

[19] P. H. Choi et al., "Side-illuminated photoconductive semiconductor switch based on high purity semi-insulating 4H-SiC," *IEEE Trans. Electron Devices*, vol. 68, no. 12, pp. 6216–6221, Dec. 2021, doi: 10.1109/TED.2021.3117535.

[20] M. Gaddy, V. Kuryatkov, N. Wilson, A. Neuber, R. Ness, and S. Nikishin, "GaN-based PCSS with high breakdown fields," *Electronics*, vol. 10, no. 13, p. 1600, Jul. 2021, doi: 10.3390/electronics10131600.

[21] V. Meyers, D. Mauch, J. Mankowski, J. Dickens, and A. Neuber, "Characterization of the optical properties of GaN:Fe for high voltage photoconductive switch applications," in *Proc. IEEE Pulsed Power Conf.*, 2015, pp. 1–4, doi: 10.1109/PPC.2015.7296862.

[22] J. H. Leach, R. Metzger, E. A. Preble, and K. R. Evans, "High voltage bulk GaN-based photoconductive switches for pulsed power applications," in *Proc. Conf. Gallium Nitride Mater. Devices*, 2013, pp. 294–300.

[23] X. Yang et al., "The initial test of a micro-joules trigger, picosecond response, vertical GaN PCSS," *IEEE Photon. Technol. Lett.*, vol. 35, no. 2, pp. 69–72, Jan. 2023, doi: 10.1109/LPT.2022.3222163.

[24] J. Huang, L. Hu, X. Yang, Y. Sun, X. Li, and C. Liu, "Modeling and simulation of Fe-doped GaN PCSS in high-power microwave," *IEEE Trans. Electron Devices*, vol. 70, no. 7, pp. 3489–3495, Jul. 2023, doi: 10.1109/TED.2023.3275115.

[25] D. Meister et al., "A comparison of the hall-effect and secondary ion mass spectroscopy on the shallow oxygen donor in unintentionally doped GaN films," *J. Appl. Phys.*, vol. 88, no. 4, pp. 1811–1817, Aug. 2000, doi: 10.1063/1.1305549.

[26] K. S. Champlin and G. Eisenstein, "Cutoff frequency of submillimeter Schottky-barrier diodes," *IEEE Trans. Microw. Theory Techn.*, vol. 26, no. 1, pp. 31–34, Jan. 1978, doi: 10.1109/TMTT.1978.1129302.

[27] K. Fujito, S. Kubo, H. Nagaoka, T. Mochizuki, H. Namita, and S. Nagao, "Bulk GaN crystals grown by HVPE," *J. Cryst. Growth.*, vol. 311, no. 10, pp. 3011–3014, May 2009, doi: 10.1016/j.jcrysgro.2009.01.046.

[28] X. Niu et al., "A photo-controlled, all-solid, and frequency-tunable ultra-wideband pulse generator," *Rev. Sci. Instrum.*, vol. 94, no. 10, Oct. 2023, Art. no. 103101, doi: 10.1063/5.0153498.

[29] Y. Zhao, Q. Wu, T. Xun, L. Wang, and H. Yang, "A scalable, general purpose circuit model for vanadium compensated, semi-insulating, vertical 6H-SiC PCSS," *IEEE Trans. Circuits Syst. II, Exp. Briefs*, vol. 68, no. 3, pp. 988–992, Mar. 2021, doi: 10.1109/TCSII.2020.3021831.

[30] M. Bora et al., "A total internal reflection photoconductive switch," *IEEE Electron Device Lett.*, vol. 40, no. 5, pp. 734–737, May 2019, doi: 10.1109/LED.2019.2903926.